Deep-Sea Research II 120 (2015) 21–34

Contents lists available at ScienceDirect

Deep-Sea Research II

journal homepage: www.elsevier.com/locate/dsr2

Entrainment induced by near-inertial drift of sea ice and its impact on under-ice biogeochemical processes in marginal ice zones

Yong Hoon Kim [a], Ho Kyung Ha [b,*], Sang Heon Lee [c], Hae-Cheol Kim [d], Hyun Jung Lee [e], Byongjun Hwang [f], Jae-Hun Park [g]

[a] RPS ASA, South Kingstown, RI 02879, USA
[b] Department of Ocean Sciences, Inha University, Incheon 402-751, South Korea
[c] Department of Oceanography, Pusan National University, Busan 609-735, South Korea
[d] IMSG, EMC/NCEP/NWS/NOAA, College Park, MD, USA
[e] Korea Polar Research Institute, Incheon 406-840, South Korea
[f] Scottish Association for Marine Science, Oban PA37 1QA, UK
[g] Korea Institute of Ocean Science and Technology, Ansan 426-744, South Korea

ARTICLE INFO

Available online 4 July 2014

Keywords:
Entrainment
Near-inertial drift
Sea ice
Marginal ice zone
Arctic Ocean

ABSTRACT

Mooring observation of hydrography, hydrodynamics and suspended particles distribution under a drifting sea ice revealed the mixing and entrainment pattern in the upper mixed layer (ML) of the marginal ice zone. The ice floe where the mooring system was installed drifted as near-inertial motion with approximately 12-h cycle. The mixing pattern induced by this near-inertial drift can be divided into two distinct regimes. First, simple entrainment (upward) fluxes from the seasonal pycnocline to sea ice–water boundary are induced by shear across ML and seasonal pycnocline during the period when ice floes drift toward pack ice. The entrainment speed was in the range of 0.25–2 m h^{-1}, which matches well with thickening and thinning of the ML during a near-inertial period. Turbulent wakes on the boundary between sea ice and open water occurred behind the advancing edge of ice. In the second regime, when ice floes drift toward open ocean, the turbulent wakes at the advancing edge of ice are combined with the entrainment caused by near-inertial motion, which results in a complex mixing pattern of both upward and downward fluxes in the ML. The echo intensity observed by the acoustic Doppler current profiler and beam attenuation from transmissometer revealed the elevated concentration of suspended particulate materials in the ML, which can be direct evidence visualizing the mixing pattern. Results suggest that the mixing and entrainment found in our study sustain particulate matters in suspension within upper ML for a few months. This may provide a potential mechanism to sustain abundant organic particulates in the ML and upper pycnocline for months after under-ice bloom. Under strong wind events like storms, the entrainment induced by near-inertial motion may also get enhanced, which causes elevated supply of nutrients from the deeper, permanent pycnocline to the ML.

© 2014 Elsevier Ltd. All rights reserved.

1. Introduction

The central part of the Arctic Ocean is known to be strongly stratified during most of seasons, in particular, even stronger during spring and summer when meltwater is supplied from sea ice (Aagaard et al., 1981; Carmack and Melling, 2011). It forms an upper mixed layer (ML) with a thickness of 20 – 100 m (e.g., Rudels et al., 1996) overlying a strong pycnocline. The primary production in the ML of the Arctic Ocean is usually limited by nutrients, especially nitrogen supply, once sufficient light penetrates to the ML during early period of ice melting seasons (Lee and Whitledge, 2005; Tremblay et al., 2006, 2008; Lee et al., 2010, 2012; Wassmann and Reigstad, 2011; Popova et al., 2010, 2012, 2013). There are two main mechanisms supplying such nutrients to the ML of the Arctic Ocean: (1) horizontal advection of nutrient-rich seawater, mostly through Pacific and Atlantic inflows (Popova et al., 2012); and (2) vertical mixing caused by winter mixing (Reissmann et al., 2009), severe storms and internal waves eroding the pycnocline (McPhee et al., 2005), wind-driven upwellings near shelf breaks and sea-ice edges (Williams and Carmack, 2008; Mundy et al., 2009; Arrigo et al., 2012), and the turbulence wake following after passage of mesoscale eddies (Smith and Niebauer, 1993). In the central part of Arctic Ocean, where there exists less chances of lateral inflow, nutrients in the ML can be supplied

* Corresponding author. Tel.: +82 32 860 7702; fax: +82 32 862 5236.
E-mail addresses: hahk@inha.ac.kr, hokyung.ha@gmail.com (H.K. Ha).

http://dx.doi.org/10.1016/j.dsr2.2014.05.019
0967-0645/© 2014 Elsevier Ltd. All rights reserved.

mostly from layers below the pycnocline through such vertical mixing processes. Studies have shown that the dynamics of the vertical mixing directly influences on the primary production in the ML (Tremblay et al., 2006, 2008; Fer and Sundfjord, 2007). Recent intercomparison study of biophysical models also shows that the vertical mixing is one of the most fundamental factors controlling primary production in the Arctic Ocean given that sea ice concentration and thickness are similar among the models (Popova et al., 2012).

The ML is usually maintained in a turbulent state by surface wind stress and/or thermal convection. The turbulence of the ML diffuses into the underlying dense homogeneous layer, resulting in the erosion of the underlying stratification via so-called entrainment (Kato and Phillips, 1969; Kranenburg, 1984; Narimousa et al., 1986; Strang and Fernando, 2001; Nagai et al., 2005). This shear-induced entrainment mechanism drives the transport of momentum, heat and materials such as salinity and nutrients between the upper ML and lower pycnocline layer (Reissmann et al., 2009). Numerous studies show that velocity shear between the upper ML and pycnocline results in entrainment of heat and salt from below the ML in Arctic Ocean (McPhee et al., 1987; McPhee and Stanton, 1996; Skyllingstad and Denbo, 2001; Skyllingstad et al., 2003). Extensive observation and model results from Surface Heat Budget of the Arctic (SHEBA) program revealed that a significant portion (ca. 20%) of ocean-to-ice heat flux was supplied by the heat entrained from layers below the pycnocline (Holland, 2003; McPhee et al., 2005; Shaw et al., 2009). Recently, Toole et al. (2010) confirmed the importance of heat entrainment into the ML and its impacts on the variation of thermohaline stratification in the central Arctic Ocean. Most of studies have stressed on moment and heat fluxes, but very few studies have been focusing on the material transport including nutrients and organic/inorganic particulate materials via entrainment.

The marginal ice zone (MIZ), the boundary between sea ice and open water, is the most active area in both physical and biogeochemical aspects (Smith and Nelson, 1985, 1986; Morison et al., 1987; Mundy et al., 2009). Arrigo et al. (2012) reported massive phytoplankton bloom under sea ice in the Arctic MIZ during 2011 summer. Their results showed that the particulate organic carbon (POC) concentration was fourfold greater in the pack ice region than in open water. They argued that nutrient upwelling to support this under-ice blooming was driven by easterly winds. However, it is rather counter-intuitive how surface wind-driven upwelling would occur in the area covered by more than 90% of thick ice. If it were not the wind-driven upwelling, then what would be the main driver for the vertical supply of nutrients in the pack ice area of the Arctic Ocean?

In this study, we propose new plausible explanation for this question. For this, we provide visual evidence that shear induced by near-inertial sea ice drift would trigger the vertical mixing and entrainment processes. We present one-day mooring data observed at the sea ice station moving along and several stationary measurements on a 550-km long transect, where vertical variability of physical and biogeochemical properties was measured. Based on the analysis of these data, we will show the direct and indirect evidences of the entrainment processes, and how they evolve over the inertial period. The entrainment speed is estimated by applying an empirical relationship between entrainment rate and Richardson number. Then, the impact of this entrainment on physical and biogeochemical processes under the ice will be discussed at the end.

2. Data collection and analysis

International Research Team led by Korea Polar Research Institute (KOPRI) conducted Arctic Ocean Research Expedition (Cruise leg: ARA02B) using IBRV *Araon*. The expedition covered deeper part of Chukchi Sea including Chukchi Plateau during July 31 – August 20, 2011 (Fig. 1). At each hydrographic station, the castings of conductivity-temperature-depth (CTD) (SeaBird, SBE 911plus) system with additional probes (e.g., transmissometer, fluorometer, oxygen sensor, etc.) were conducted to measure the profiles of temperature, salinity, and other biochemical parameters.

Water samples for chlorophyll *a* (Chl-*a*) and nutrient concentrations were collected from standard depths (0, 10, 20, 30, 50, 80,

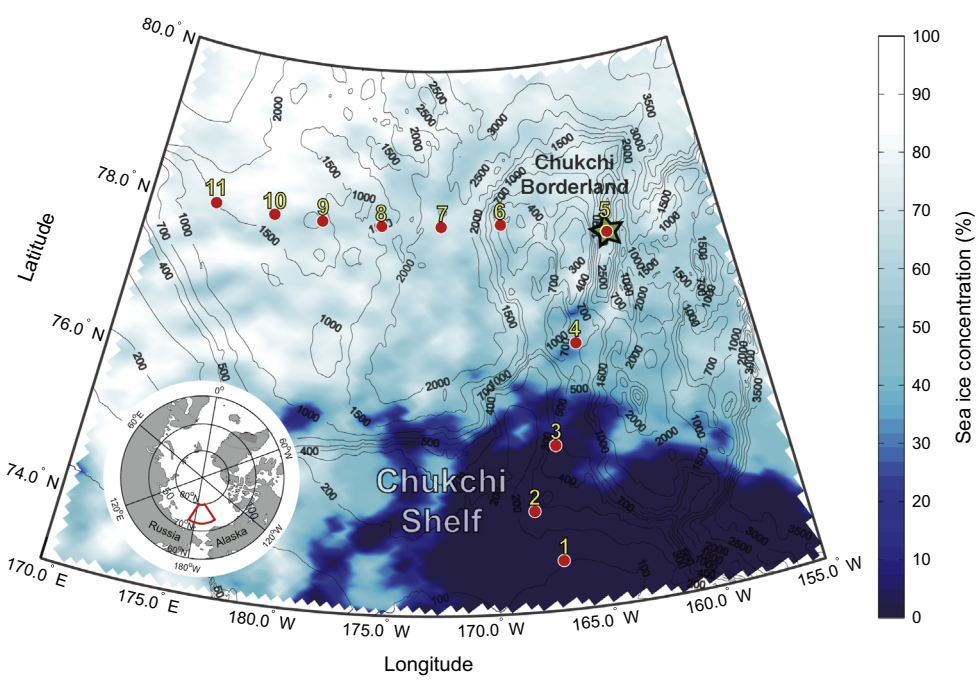

Fig. 1. Study area with bathymetry (in meter) overlain on the sea ice concentration on August 7, 2011 (Cavalieri et al., 2011). Numbers indicate the station numbers. The star indicates the initial position of sea ice experiment site.

100, and 150 m) using a Rosette sampler equipped with twenty 10-l-Niskin bottles at each CTD station. Water subsamples (0.3 – 0.5 l) for measuring Chl-*a* concentration were filtered onto Whatman GF/F filters (diameter: 24 mm). The filters were kept frozen until onboard analysis using a Trilogy fluorometer (Turner Designs Inc.) which had been calibrated with commercially purified Chl-*a* preparations. The methods and calculations for Chl-*a* were based on Parsons et al. (1984). Major dissolved inorganic nutrients (nitrite + nitrate, silicate, and phosphate) were analyzed onboard using a Bran and Luebbe model Quatro auto analyzer (SEAL Analytical, UK), according to the manufacturer's manual.

For monitoring the dynamic motions of sea ice and water in the ice-ocean boundary (i.e., upper ML), a tripod was installed on the surface of sea ice station (St. 5 in Fig. 1). An ice hole was made on the ice floe, which was located several hundred meters away from the ice floe edge. An acoustic Doppler current profiler (ADCP) (Teledyne RDI, 600 kHz) was mounted on the tip of vertical extension arm of a tripod at 3.6-m depth below the water surface. The orientation of ADCP was fixed with respect to the ice floe, and thus when the floe rotated the ADCP rotated the same amount. However, the current velocities were measured as earth-coordinate by using internal compass in the ADCP. The ping rate was 1 Hz, and 1-min ensemble average was continuously recorded. ADCP data were collected every 1 min, and the data were post-processed by using WinADCP® provided by Teledyne RDI. All the data were low-pass filtered with 1-h window, and these filtered data were used for further analyses including estimating friction velocity. In addition, the current velocities were converted from the ones relative to ice (relative velocity hereafter) to the absolute velocity by adding ice velocity (see Ha et al. (unpublished data) for details). ADCP data collection started on 08:45 GMT, August 7 and ended at 07:32, August 8, 2011, covering slightly less than 24 h. Right next to the ADCP location, a total of 8 CTD casts were conducted between 18:20, August 7 and 06:30, August 8, 2011 with every 2-h interval. Due to in-situ undesirable conditions, unfortunately, the CTD casting had not been conducted during the first 9.5 h.

A Sea Ice Mass Balance Array (SIMBA; SAMS, 2010) was also installed near the tripod where the ADCP was installed. A SIMBA consists of a thermistor string (about 5-m long), a Global Positioning System (GPS) and Iridium transmitter and receiver. Ha et al. (unpublished data) described the details of this sea ice experiment.

3. Results

3.1. Hydrographic characteristics of the study region

The hydrography in the study area (Chukchi Borderland/Chukchi Shelf) is characterized by four distinct water masses: (1) Surface mixed layer water (SMLW); (2) Pacific summer water (PSW); (3) Pacific winter water (PWW); and (4) Atlantic water (AW) from top to the bottom. SMLW has the lowest salinity (down to about 25 psu) due to the sea ice melting and lateral freshwater input (Fig. 2). PSW is relatively warmer and fresher water mass, but saltier than SMLW. Its salinity is in the range of 30 – 32 psu, and temperature is around −1.5 to 0.2 °C (Fig. 2). PWW, a layer of relatively fresh (i.e., buoyant), cold water, lies immediately above the AW with the highest temperature and salinity. PWW plays a role in shielding the exchange of heat flux between overlying PSW and underlying AW. In this study, we focus on SMLW and PSW mostly.

The vertical profiles measured from ship-operated CTD castings are selectively presented in Fig. 2. The surface salinity and density were as low as 26.2 psu and 1021 kg m^{-3}, which is attributed to the summer melt of sea ice. The near-surface temperature was slightly higher than the freezing temperature, and the maximum was recorded at a depth of 30 – 50 m. For instance, the warmest water (0.2 °C) was found at 44 m.

The upper layer above 5 – 10 m was isolated due to a strong pycnocline, the thickness of which ranges up and down among stations. At this juncture, it should be noted that the three stations are geographically close to each other (approximately 1 km apart), and ~6 h time span between St. 5-1 and 5-2 and ~1 h between St. 5-2 and 5-3. Further below this strong pycnocline, the second pycnocline was observed around 30 – 40 m where the top of the maximum temperature layer was placed (Fig. 2). A lateral transect along the 78 °N, the second pycnocline was deeper in the east of the transect and became shallower up to ~20 m toward the western end (Fig. 3a). The warmest water mass existed in the eastern flank of Chukchi Plateau, and the maximum temperature (> 0 °C) was found at about 50 m below the second pycnocline (Fig. 3a). The signal of warm temperature gradually diminished toward the west. The low-density (< 1023 kg m^{-3}) water produced by sea ice melting was developed on the eastern section, which is the MIZ.

The elevated fluorescence signals were observed at depths of 40 – 50 m on most of stations, coincident with upper part of lower pycnocline (Figs. 2 and 3). This fluorescence signal was correlated well with the distribution of Chl-*a*, which is so-called subsurface chlorophyll maximum (SCM) and will be discussed in detail later. Its depth also matched well with the peak of beam attenuation (Figs. 2 and 3f), probably because most of suspended materials are composed of the biogenic matters such as phytoplankton. In addition to SCM depth, second or third peaks were also observed in the beam attenuation. Those peaks were generally located in the ML (i.e., around the shallower pycnocline and above), which sometimes showed even stronger signal than SCM peak (e.g., St. 11 in Fig. 3f).

Fig. 3 shows the summary of physical and biogeochemical conditions along the transect that includes the ice station in the eastern end (see Fig. 1 for the location of the transect). In general, Chl-*a* concentration was low (< 0.1 μg l^{-1}) throughout the water column except the SCM layer which was ubiquitously formed at a depth between 25 and 50 m (Fig. 3b). Chl-*a* concentration at the SCM ranged from 0.4 to 0.9 μg l^{-1}, with an average of 0.6 μg l^{-1}. The major nutrient concentrations were very low at the surface ML between surface and about 30-m depth, and then rapidly increased down to the depth with maximum concentration (Figs. 3c–e). The concentration of NO_2+NO_3 ranged from 0 to 16.1 μM within the euphotic layer (< 100 m), and mostly depleted in the upper ML (< 30 m; Fig. 3c). The concentrations of SiO_2 and PO_4 were in the ranges of 3.0 – 30.8 μM and 0.6 – 2.1 μM, respectively (Figs. 3d and e).

3.2. Measurements on the ice station

Since we aimed at the MIZ, our cruise started from the Chukchi Shelf toward the north until we found ice packs that are suitable for the observation platform (Fig. 1). It was over 90% of ice covered in the area where we installed the ADCP mooring. The low salinity in the ML indicates that ice melting is active in this region (Fig. 2). Fig. 4 shows the velocities estimated by the ADCP installed on the ice floe, which were relative velocity to the platform before post-processing. North–South (N–S) and East–West (E–W) components of velocities exhibited a distinct temporal variability of ~12-h cycle caused by the near-inertial motion of sea ice. An interesting feature in the velocity structure is vertical variability, whereby a strong velocity shear was observed at ~12 m below the surface (Figs. 4 and 5). Surface currents relative to sea ice were quite slow, and got stronger below the shear layer. For instance, the velocities

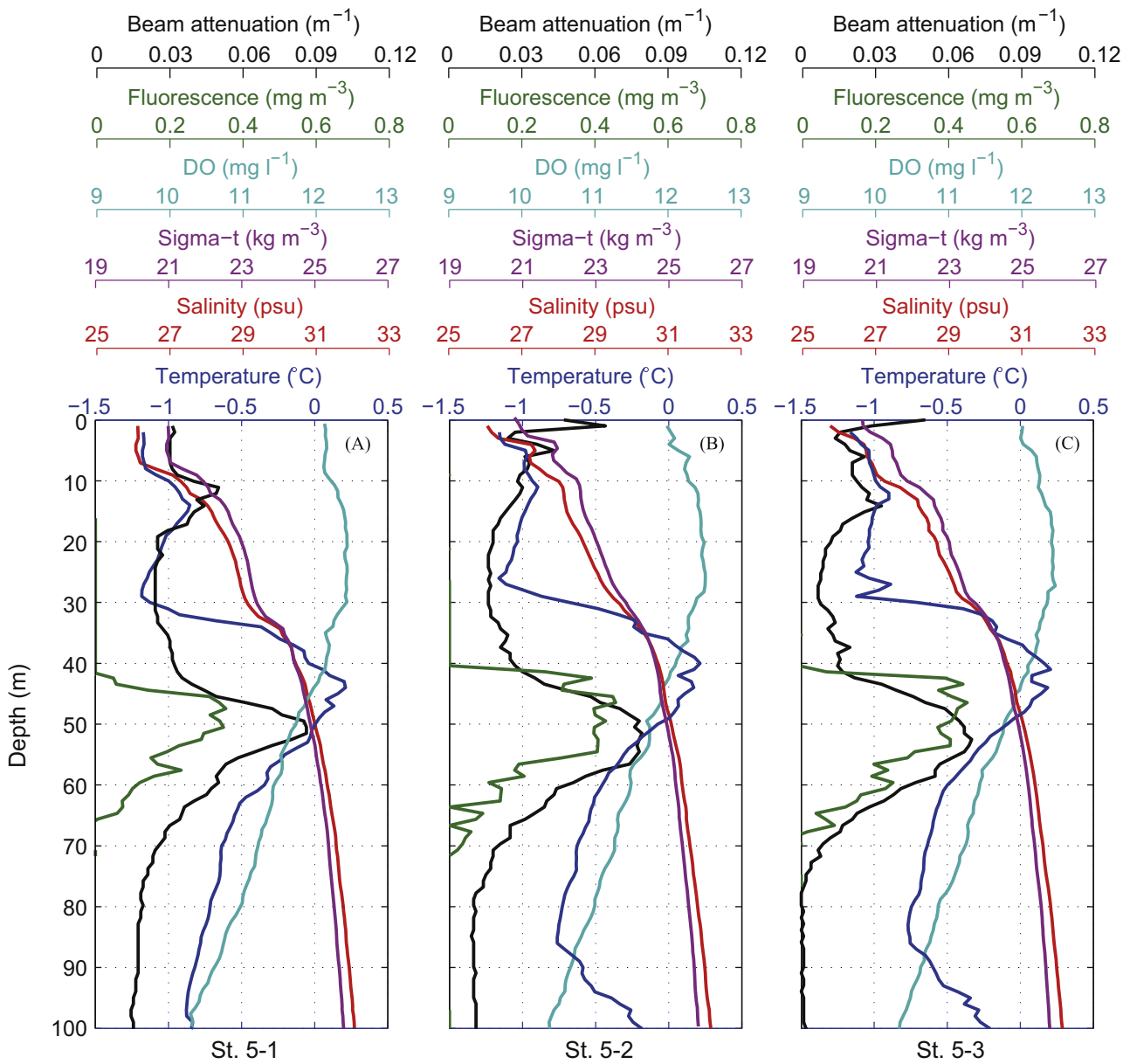

Fig. 2. Representative vertical profiles of ship-board CTD near the ice mooring station (St. 5). It is noted that three stations are located within 1-km distance, and there is about 6 h time span between St. 5-1 and 5-2, and 1 h between St. 5-2 and 5-3.

at the near-surface (5.1-m depth; 4th bin) and below the shear layer (13.9-m depth; 48th bin) showed the clear difference in the current pattern between surface and deeper layers (Fig. 4c and d). When the current pattern in the deeper layer is compared with the velocity derived by ice drift of SIMBA (Figs. 4d and 6a), one may note that the currents observed in the deeper layer were opposite to the ice drift velocities, while the magnitudes of those two were very similar. In addition, the currents relative to the ice drift were almost zero in the layer close to ice–water boundary (Fig. 4c). Another characteristic feature is that the magnitudes of both N–S and E–W components became smaller toward the ending period of observation (Figs. 4c and 4d).

Strong shear between the upper and lower layer in N–S and E–W components also indicates that the direction of the relative currents varies vertically. For instance, the surface current at 12 h ('hr' represents elapsed hours after 00:00 GMT, August 7 hereafter) was directed to N in the upper layer but toward NE in the deeper layer, showing counterclockwise rotation with depth (Figs. 5a and b). This change in speed and direction occurred around 12-m depth during most of the observation period (Figs. 5c and d). However, the depth of shear boundary in the upper and lower layers also became shallower toward the ending period of the near-inertial oscillation, e.g., during 12 – 14 h and 25 – 28 h (Figs. 4a and b).

Fig. 6 shows the drift velocity of sea ice estimated from SIMBA (Fig. 6a) and the acoustic echo intensity (Fig. 6b). The ice floe was drifted with the maximum speed of 0.33 m s^{-1}. The first order signal was near-inertial drift with 12-h cycle, with acceleration phase in drift speed during 9 – 14 h and 20.5 – 27 h and decelerating drift speed during 14 – 20.5 h and 27 – 32.5 h (black solid line in Fig. 6a). As expected, the drift was clockwise changing from W-, N-, E-, and then to S-ward direction, which is a typical sign of near-inertial drift in northern hemisphere. The background ocean current was directed to the NE, so that the N and E components of ice drift velocity were larger than the S and W components (Fig. 6a).

Echo intensity, as a proxy for suspended materials (see Ha et al., unpublished data), shows similar trends of 12-h variability but a bit more complicated (Figs. 6b and 7). During the period when the

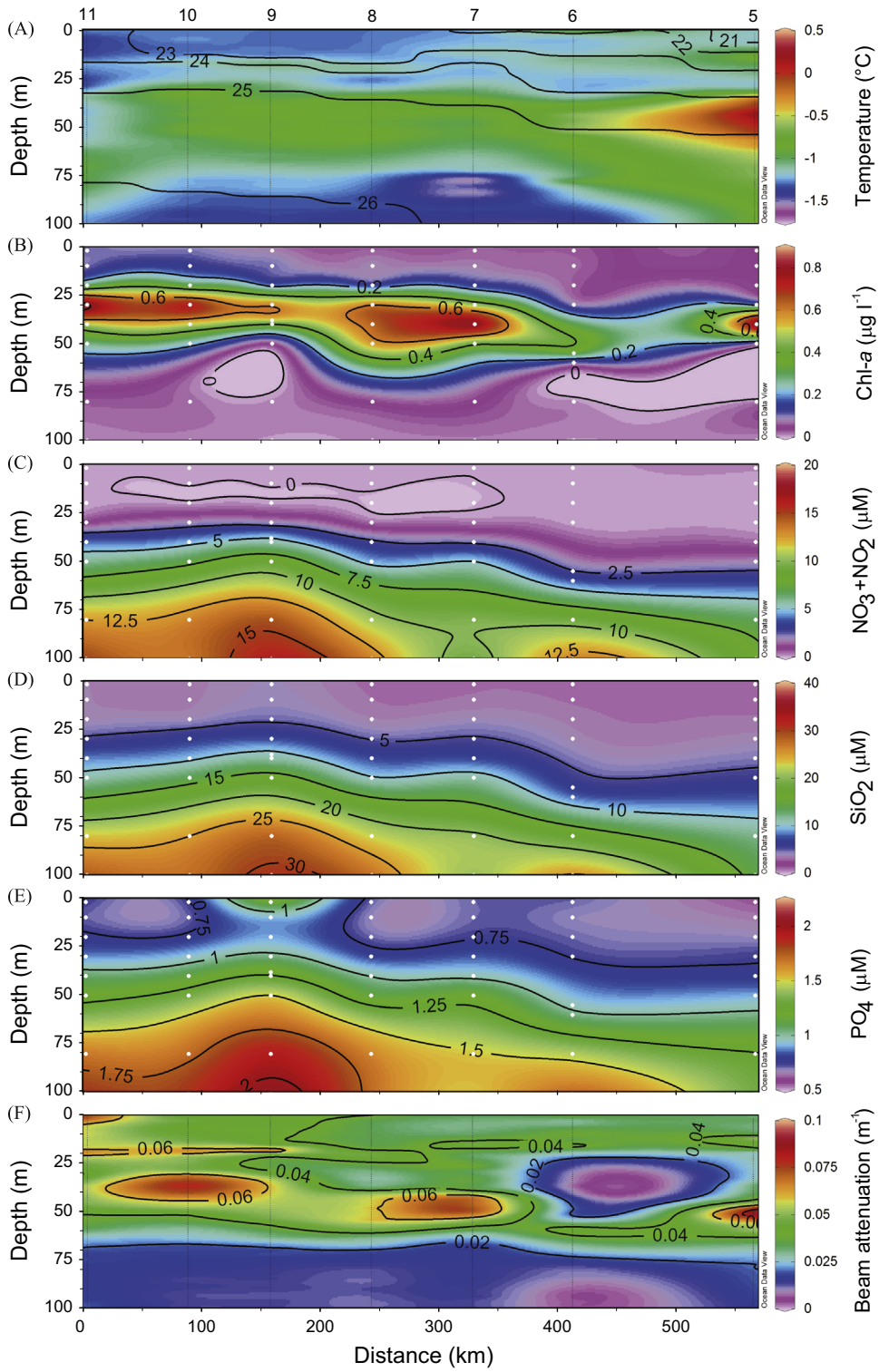

Fig. 3. Cross-sections of (A) temperature with the isopycnal (sigma-t, contour); (B) Chl-*a*; (C) NO_2+NO_3; (D) SiO_2; (E) PO_4; and (F) beam attenuation. Station numbers are shown on the top of panel (A). White dots are the sampling depths. Each panel was prepared with ODV software (odv.awi.de).

drift velocity increased (i.e., 9–14 h), the elevated echo intensity was observed throughout the entire water column (Figs. 6b and 7a). During the first 3 h of observation (9 – 12 h), the layer with high echo intensity exhibited a complex fluctuation pattern in both upward and downward movement with the time. For instance, a layer detected at 7.5 m at 9 h was relatively stable for an hour, and then lowered to 9 m until 11 h with a high-frequency fluctuation (a few to tens of minutes). On the contrary, a layer with elevated echo intensity detected near 13 m at 9.5 h moved upward to 11 m at 11.5 h, and was eventually crossed with the downward signals around 11.5 h (Figs. 6b and 7a). After 11.75 h, upward movements of the higher echo signal layer were detected in the upper part of the ML. There exists wave signal of ~5 m wave height (e.g., between 7 and 12-m depth) and 20 – 30 min of wavelength during 11.5 – 13.5 h, which may indicate the presence of internal waves. High-frequency internal waves were also active

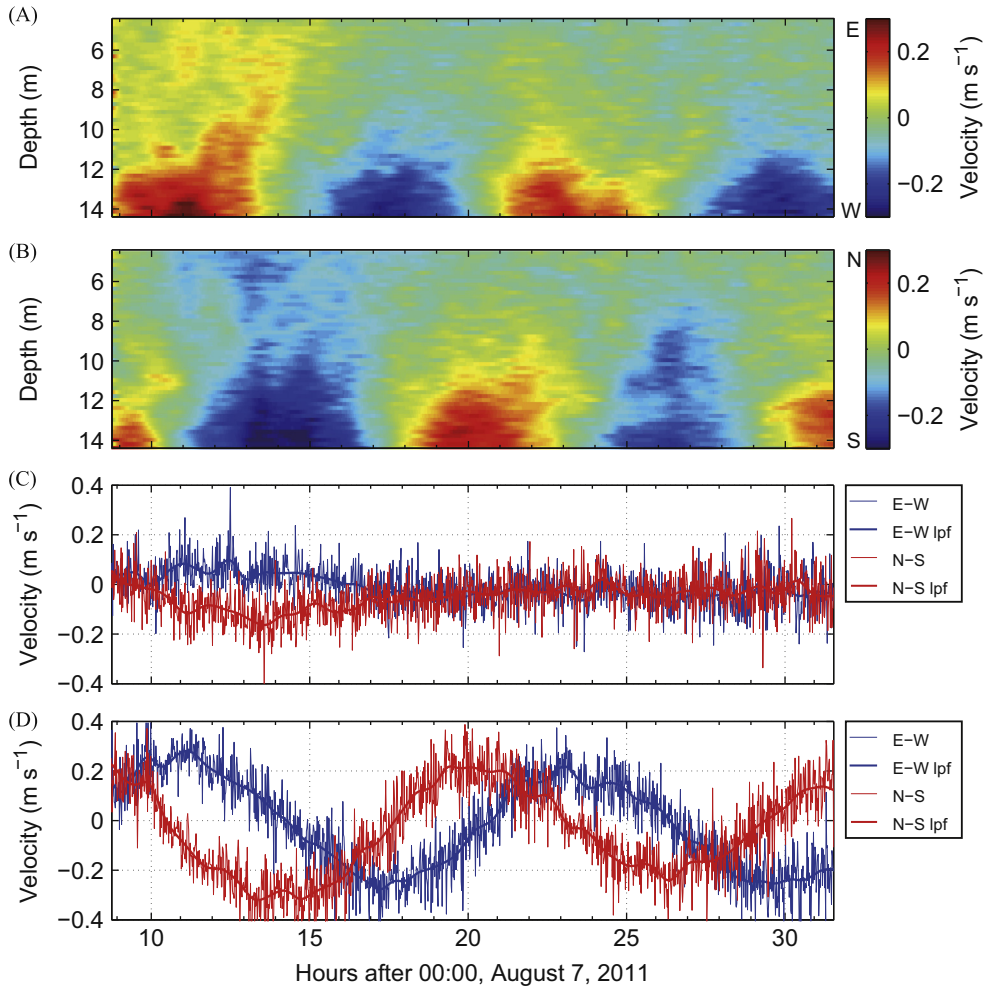

Fig. 4. Moored ADCP data at sea ice floe: (A) E–W and (B) N–S components of velocity profiles; (C) velocities at 5.1 m; and (D) 13.9 m. All the velocities are presented as relative to ice. 1-h low-pass filter (lpf) was applied to remove the noises.

at 6-, 10-, and 12-m depth during 14 – 15.5 h (Fig. 6b). This complicated mixing pattern of elevated suspended materials, which is caused by the upward and downward fluxes and active internal waves, occurred while ice was being drifted toward NW and N directions (Fig. 7a).

During 14 – 16 h when the ice drift speed reached the maximum, water masses with relatively lower concentration of suspended materials were observed at 11-m depth and below (Figs. 6b and 7b). This layer moved upward to 7-m depth until 18 h. In addition, another upward movement of relatively higher intensity layers was observed from 13- to 6-m depths during 16 – 20 h (Fig. 6b). These upward fluxes were accompanied by high-frequency internal waves, but the signal strength was relatively lower compared to the period when complicated fluxes occurred. This clear upward flux happened during the period when ice floe was being drifted toward NE, E, and then SE (Figs. 7a and 7b).

During 21 – 31.5 h of the second near-inertial drift period, similar vertical flux pattern was observed in the echo intensity. For 21 – 25 h, the complicated upward and downward fluxes were present, followed by stable layers with high intensity of internal wave signal (Figs. 6b and 7a). Then, relatively weak echo intensity layer was observed at 10-m depth and below (28 – 29 h), which migrated upward for the next several hours.

The 3-D plots in Fig. 7 show the spatial and temporal relationship between ice drift and echo intensity, with respect to the difference between the first and second half of the near-inertial period. For the first half (9 – 14 h and 21 – 26 h) of near-inertial drift circle, when the ice floe was drifted toward W and NW, higher echo intensity was detected. During this period, the mixing was dominated within most of the ML (Fig. 7a). On the other hand, the echo intensity was relatively lower, and a clear upward flux was observed during the second half (14 – 20 h and 26 – 30 h) of near-inertial drift circle (Fig. 7b). It is noticed that high frequency internal waves were more active during the period when the ice floe was drifted toward the north with a maximum speed.

The temporal variability of hydrographic structure is shown in Figs. 6c and d. A strong halocline was found around 12 m, which fluctuated over time. Its depth was the shallowest at 12 h when the ice drift speed was relatively small. The pycnocline became deeper by ~1 m during acceleration period of the near-inertial period and bounced back to similar depth after 12-h cycle. More details in vertical structure before and during the ice station can be seen in Fig. 8. Within top 20-m water column, the temperature maximum was observed at a depth of 13 – 15 m. The pycnocline was abruptly lifted up to 6-m depth on 7.4 h before 00:00 GMT, August 7 which was from ship-casted CTD before the installment of ice station (Fig. 8). One may concern about the effect of stirring caused by the ship on the structure of the upper water column. However, hydrography data from the uppermost layer (< 5 m deep) of the three ship-casted CTD profiles (– 12.7, – 7.4 and – 6.3 h) are reasonably consistent with those of ice station CTD data, and the most noticeable difference of temperature and salinity occurred at 5 – 12 m depth.

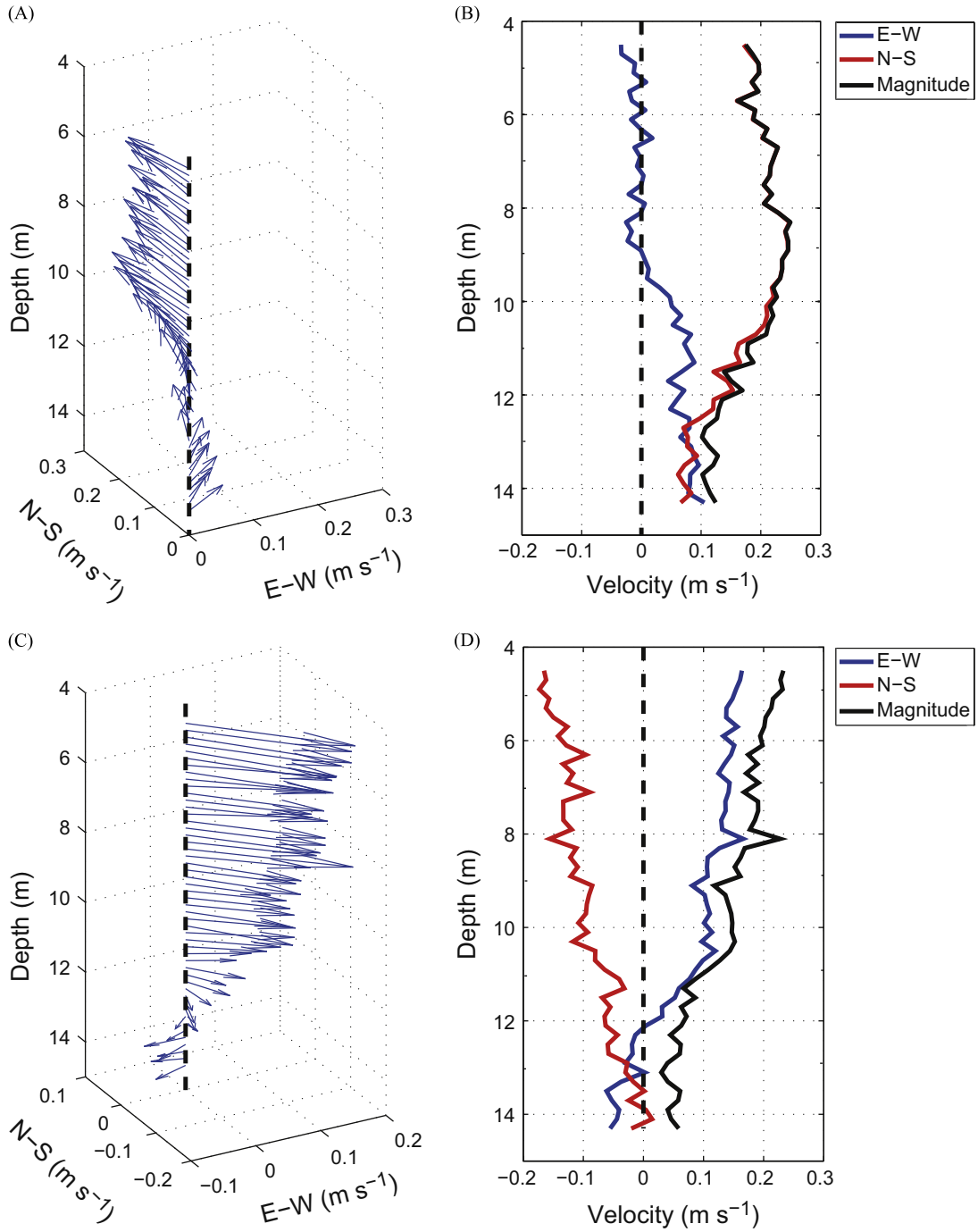

Fig. 5. (A) 3-D structure of the current vectors averaged during 12 – 12.5 h; (B) same as (A) with decomposed into E–W and N–S components; and (C, D) same as (A, B) but during 18 – 18.5 h.

Thus, we concluded that this is not influenced by the ship stirring or any artifact of sampling methodology.

4. Discussion

4.1. Mixing and entrainment mechanism associated with near-inertial motion

Two distinct pycnoclines were recognized in our transect: one being at ~10 m and the other around 30 – 40-m depth (Figs. 2 and 3). The upper one can be regarded as seasonal pycnocline that is closely related to ice melting. A stronger mixing stirs water column above this pycnocline, which destratifies water in the ML. Below the seasonal pycnocline, the water column is stably stratified with abrupt increase in both salinity and temperature around 30 – 40-m depth. This lower pycnocline is the upper bound of warmer water mass with high nutrients (nitrate in particular), and elevated concentration of Chl-*a* (see Fig. 3). Higher temperature and relatively lower salinity (30 – 32 psu), in spite of salinity being higher than that in the upper ML, indicates that this water is originated from the Pacific, and that the lower pycnocline is thought to be a permanent pycnocline. Since we focus on the processes in the upper ML, the pycnocline we refer in this paper without any explanation would be upper, seasonal pycnocline hereafter.

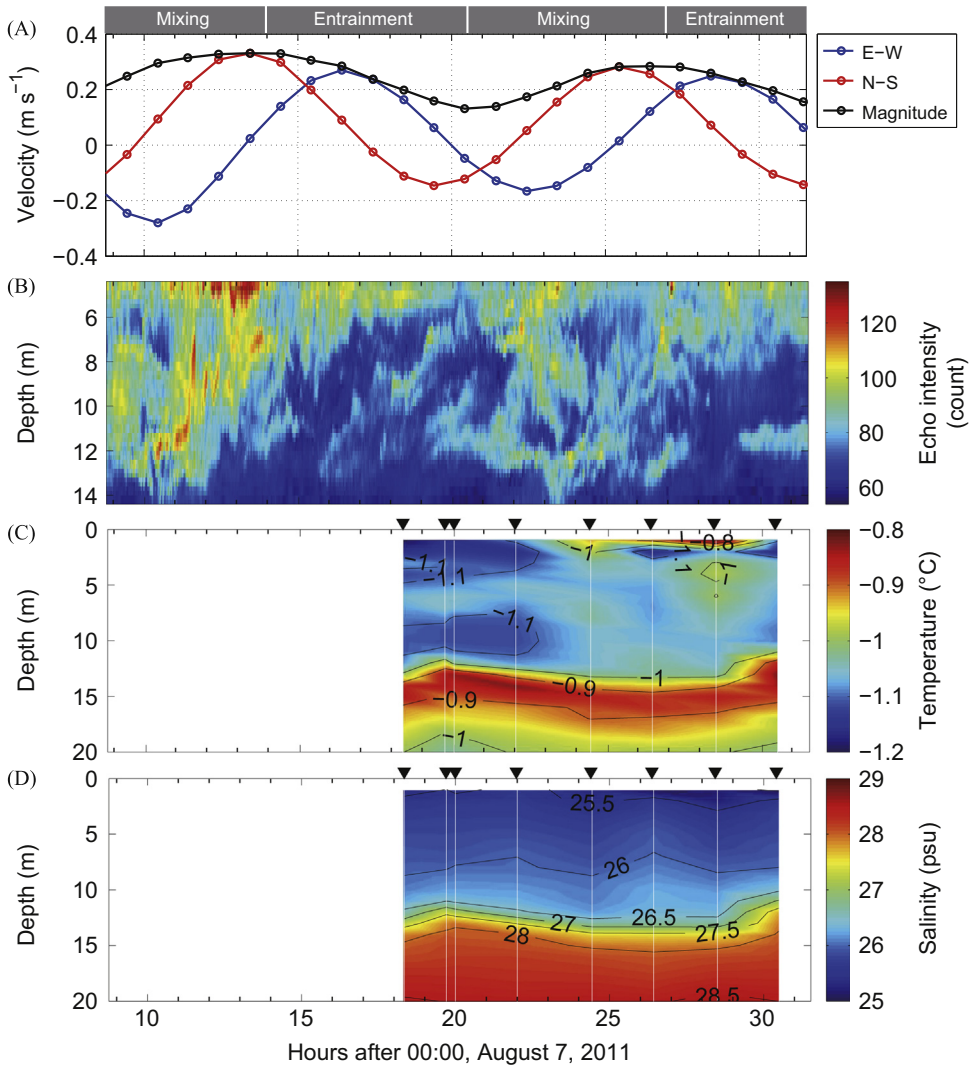

Fig. 6. Moored data at sea ice floe: (A) drift velocity of sea ice estimated from SIMBA. Positive represents E and N, respectively; (B) acoustic echo intensity; (C) temperature; and (D) salinity. Triangles on the top of (C) and (D) indicate the timing of CTD casts.

The ice drift and currents during our observation periods are strongly driven by near-inertial motion. Many studies reported observation of near-inertial drift of ice floes and its impact on mixing in the ML (e.g., McPhee, 1978, 1980; Morison et al., 1987; McPhee, 1992), so it is not completely unexpected phenomenon in the central Arctic Ocean. A strong wind event (> 15 m s^{-1}) was observed 3 days before ice station experiment (not shown here), which might have triggered the near-inertial motion. This implies that the ice experiment period occurred during the relaxation period, that is probably why the magnitude of inertial speed of ice decreases gradually (Fig. 6a). Vertical shear near the upper pycnocline is associated with stronger currents in the upper ML and slower flows below the pycnocline (Figs. 4 and 5). This indicates that the movement of the upper ML is synchronized with the movement ice floes, a similar condition in an ice-slab model with higher drag coefficient between ice and water (e.g., Skyllingstad and Denbo, 2001).

Another characteristic feature is the counterclockwise or clockwise rotation of the relative (corrected) currents with depth, which would be a clear signal of Ekman spiral (e.g., McPhee and Martinson, 1994). The comparison between velocity structure and hydrography for the second half of observation period suggests that the depth where velocity shear occurs coincides with that where the counterclockwise rotation starts (see Fig. 5). This implies that the speed and direction of currents significantly change across this pycnocline. During the early stage of observation (12 – 14 h), this boundary of velocity shear and rotation moved up from 12- to 6-m depth (Figs. 4a and 5a), which may indicate the uplift of the pycnocline and the thinning of the ML. Although no ice-based CTD data are available during that period, ship-board CTD data at approximately 12 h before the ice station (e.g., St. 5-2 and 5-3) showed that the pycnocline was located around 5-m depth (Fig. 8), supporting our findings.

Vertical and temporal variability in echo intensity reveals two distinct mixing processes in the ML during a cycle of near-inertial ice drift. First, particulate materials were transported gradually upward from the seasonal pycnocline (~12–14-m depth) to the upper ML (~6-m depth) in a few hours (Fig. 6). This phenomenon was observed during a waning period of near-inertial ice drift speed, i.e., the second half of drift circles (Figs. 6 and 7). During this period, ice floe drifted toward NE or E. The TerraSAR-X ScanSAR image taken a day before our observation shows that the edge of ice packs are aligned NW–SE direction, with open lead located in the SW of ice packs. NE/E movement of ice indicates that the ice floe with our mooring is moving toward ice pack areas from open water, and thus our observation data represent the mixing regime of leading edge of ice floe. Using a Large Eddy Simulation (LES), Skyllingstad and Denbo (2001) demonstrated

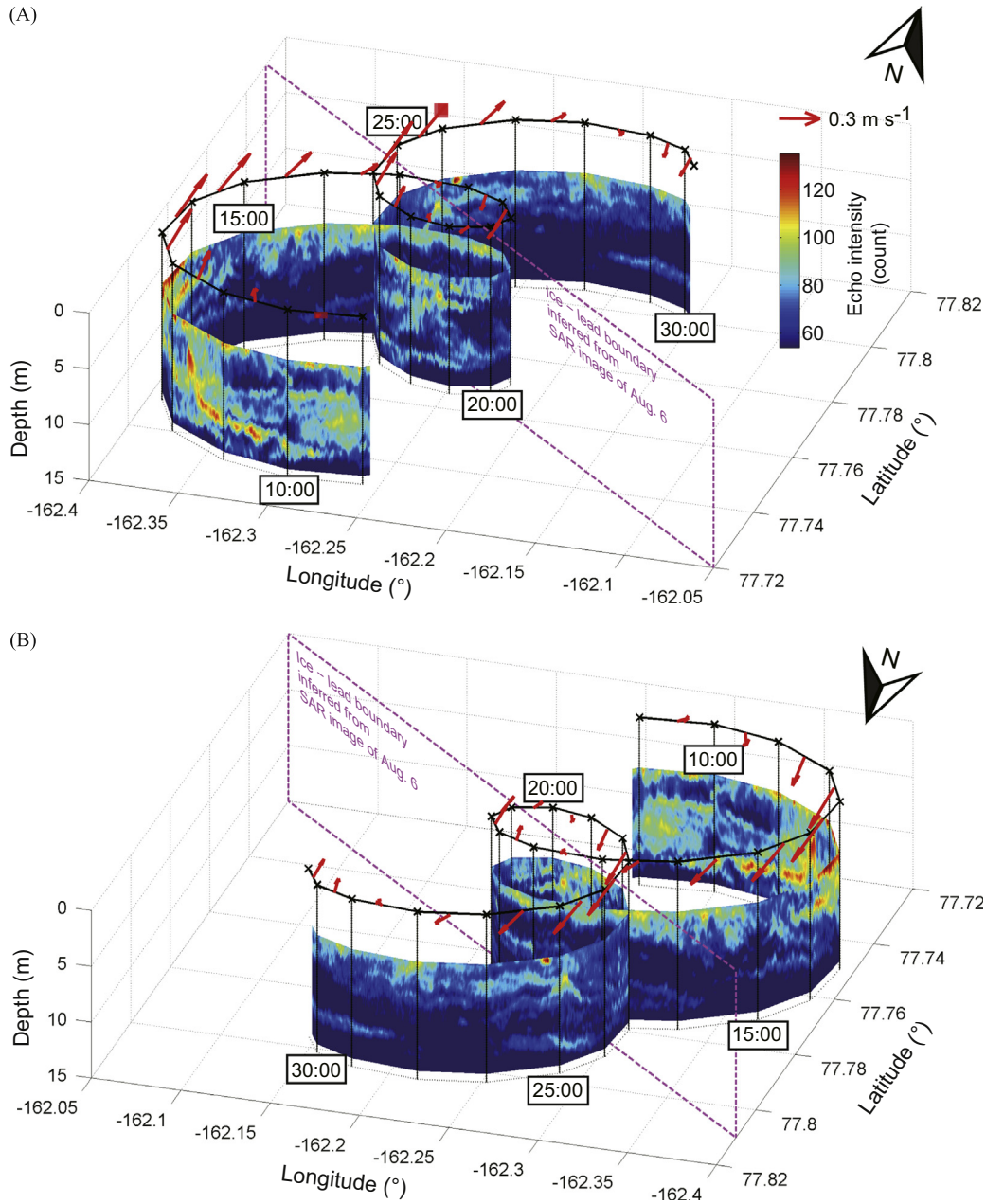

Fig. 7. (A) Near-inertial motion of sea ice floe and acoustic echo intensity during the mooring campaign with the camera view from south to north, (B) same as (A) but view from northwest to southeast to show the opposite side of (A). Thick black line at the surface show the track of ice floe and red arrows represent ice movement. Thin vertical lines are time tick for every hour with numbers representing hours after 00:00 GMT, August 7, 2011. The magenta dashed box indicates the ice-lead boundary from TerraSAR-X ScanSAR image (see Ha et al., unpublished data). (For interpretation of the references to color in this figure legend, the reader is referred to the web version of this article.)

how the leading edge of ice floe generates mixing in the ML, which causes vertical entrainment of water from the pycnocline. It is however noted that their ice motion was even half time slower than what observed in this experiment, so we can expect more effective entrainment in our case (Fer and Sundfjord, 2007).

The other type of vertical mixing exhibits more complicated pattern of upward and downward fluxes of suspended materials (e.g., 10 – 16 h in Fig. 6). This phenomenon is typically observed during the first half of near-inertial drift (Figs. 6 and 7). This period represents the acceleration phase in near-inertial cycle, when ice drifted to W/NW. As the advancing edge of ice pack faces open water, representing trailing edge of ice pack on our observation station. Also, during the beginning part of the near-inertial circle, the ice floe returned to the same area where the ice floe stayed during the second half of the previous cycle (see Fig. 7). This indicates that complicated mixing pattern might be associated with the combined dynamics of both the advancing and trailing edges of the ice floe. The difference between two mixing patterns, entrainment vs. turbulent mixing, is clearly seen during 18 – 24 h in Figs. 6 and 7. Although the observation station covers almost the same track between 18 – 21 h and 21 – 24 h in less than 1 km apart, the mixing pattern between these two periods is significantly different whereby a simple, clear upward fluxes during 18 – 21 h vs. both upward and downward fluxes during 21 – 24 h.

Schematic diagrams shown in Fig. 9 illustrate the oscillatory feature of mixing and entrainment patterns. When an ice floe drifts toward ice pack (i.e., leading edge of ice), the shear across the pycnocline increases which generates entrainment from the pycnocline below (Fig. 9a). Turbulent wakes are generated behind the advancing ice edge. Thus, our observation only captured steady

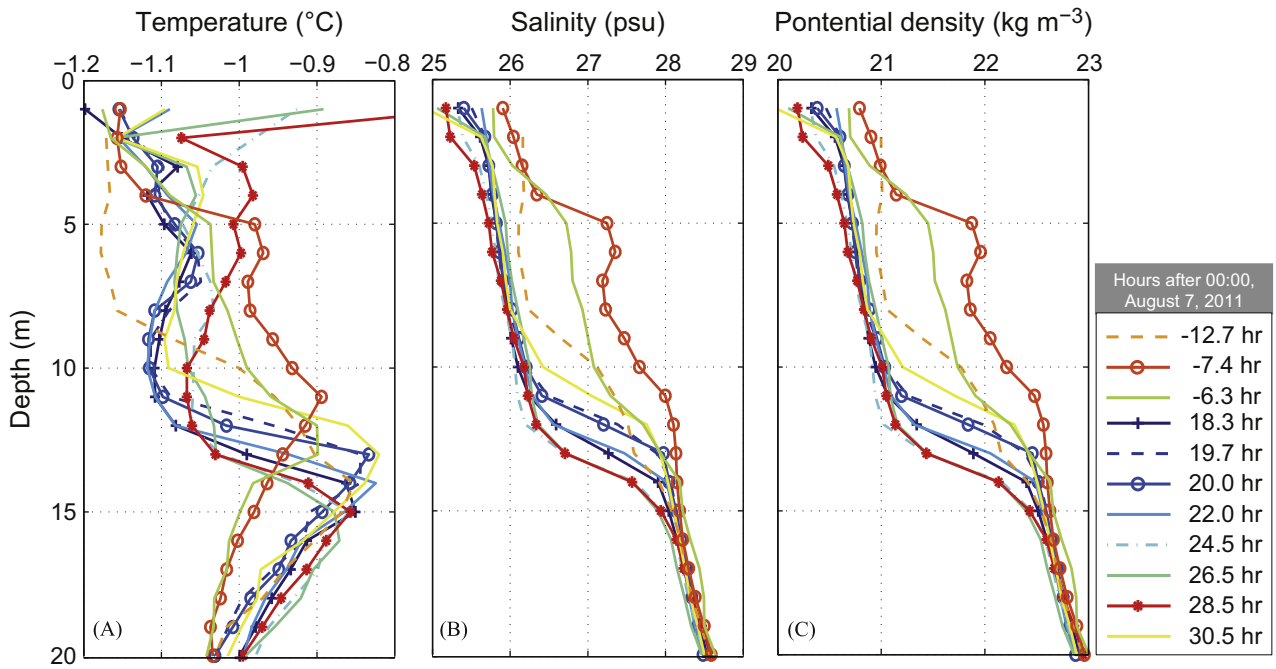

Fig. 8. Vertical CTD profiles sequentially measured at sea ice station (St. 5): (A) temperature; (B) salinity; and (C) potential density. It is noted that the pycnocline was abruptly lifted up to 6 m on −7.4 h.

upward fluxes due to the entrainment. Continuous entrainment may result in thickening the ML, which was confirmed by the vertical profiles of CTD data. On the other hand, when an ice floe moves toward open waters, turbulent mixing generated at the advancing ice edge is combined with upward fluxes due to entrainment by shear (Fig. 9b). In our cases, this mixing period was also overlapped with the remnant entrainment fluxes in the previous inertial oscillation (i.e., in the overlapped circle during 18 – 24 h in Fig. 7). In addition, the leading edge would experience less drag than the opposite case because the strength of the stabilizing influence depends on the temperature difference across the boundary layer and advancing ice cools the water behind it (McPhee, 1983). This may augment the asymmetric pattern of mixing during inertial oscillation near the ice edge.

Entrainment rate is one of key parameters in characterizing the entrainment phenomenon at the interface of a stratified fluid. Laboratory experiments have suggested a power law relationship between the entrainment rate, defined as the entrainment speed (U_E) normalized by the friction velocity (u_*), and the bulk Richardson number (Ri_*) (Kato and Phillips, 1969; Kranenburg, 1984; Narimousa et al., 1986; Strang and Fernando, 2001),

$$\frac{U_E}{u_*} = c(Ri_*)^{-m} \tag{1}$$

where $Ri_* = h\delta b/u_*^2$, h is the depth of the mixed layer, $\delta b = g\delta\rho_0$ is the buoyancy difference, $\delta\rho$ is the density difference between the two layers, ρ_0 is the reference density and g is gravity. c and m are constants and vary with the Richardson number, the ratio of potential to kinetic energy. For example, when Ri_* approaches zero, the interface becomes more turbulent, and the U_E becomes proportional to u_*. When Ri_* approaches the infinite, on the other hand, the interface becomes stable, and turbulent eddies are not strong enough to entrain against gravitational forces. As a result, U_E must be near-zero value, and m becomes large. In fact, values suggested for m range from 0.5 (Price, 1979; Kranenburg, 1984; Narimousa et al., 1986) to 1.0 (Kato and Phillips, 1969; Narimousa et al., 1986).

By applying the logarithmic law of the wall to our corrected ADCP velocity (i.e., absolute velocity), the friction velocity in the ML, u_* is found to be ranging 0.01–0.02 m s^{-1}, which is consistent with the values reported in the Arctic Ocean (McPhee, 1983, 1987, 1994, 2002, 2004). The density profiles measured and the depth of mixed layer of ~10 m are used to estimate Ri_*, which is in the range of 240 – 950. This is comparable to the values reported by laboratory experiment (Narimousa et al., 1986) and field data (Nagai et al., 2005). Narimousa et al. (1986) and Strang and Fernando (2001) suggested that under these range of Ri_* the Kelvin–Helmholtz type instabilities appear and the entrainment is slower than the fully turbulent eddies with $m=1$ and $c=7$ for Eq. (1) (Narimousa et al., 1986). Thus, U_E is found to be $0.07 - 0.57 \times 10^{-3}$ m s^{-1} (=0.25 – 2.0 m h^{-1}). With 6 h of entrainment period (i.e., half of near-inertial cycle), the change in the depth of ML can be between 1.5 and 12.4 m that is consistent with our findings. Fer and Sundfjord (2007) reported that the entrainment rate, U_E/u_*, is rather constant (0.014) with relatively lower values of Ri_* (< 10) in the MIZ of the eastern Arctic. If we apply this relationship with our friction velocity range, the entrainment speed is found to be $0.14 - 0.28 \times 10^{-3}$ m s^{-1} (=0.5 – 1.0 m h^{-1}), which is also within the range estimated above.

4.2. Physical implications of the entrainment

The entrainment effect during near-inertial oscillation may induce thickening of the ML as warmer and saltier water from the pycnocline below enters into the ML and vice versa. Although our CTD profiling spans only a single cycle of inertial drift, the observation clearly shows two opposite cases: (1) uplift of pycnocline (i.e., thinning of the ML) in the acceleration phase of inertial cycle and (2) lowering of pycnocline (i.e., thickening of the ML) in the deceleration phase of inertial cycle. The velocity shear and rotation observed from ADCP exhibit the same oscillatory behavior. Interesting feature is that the ML depth (inferred from the location of vertical shear boundary) moves only 1 – 2 m up and down during the second inertial cycle (20 – 31 h), but it fluctuates up to 5 m for the first inertial cycle (9 – 20 h in Figs. 6 and 8). CTD

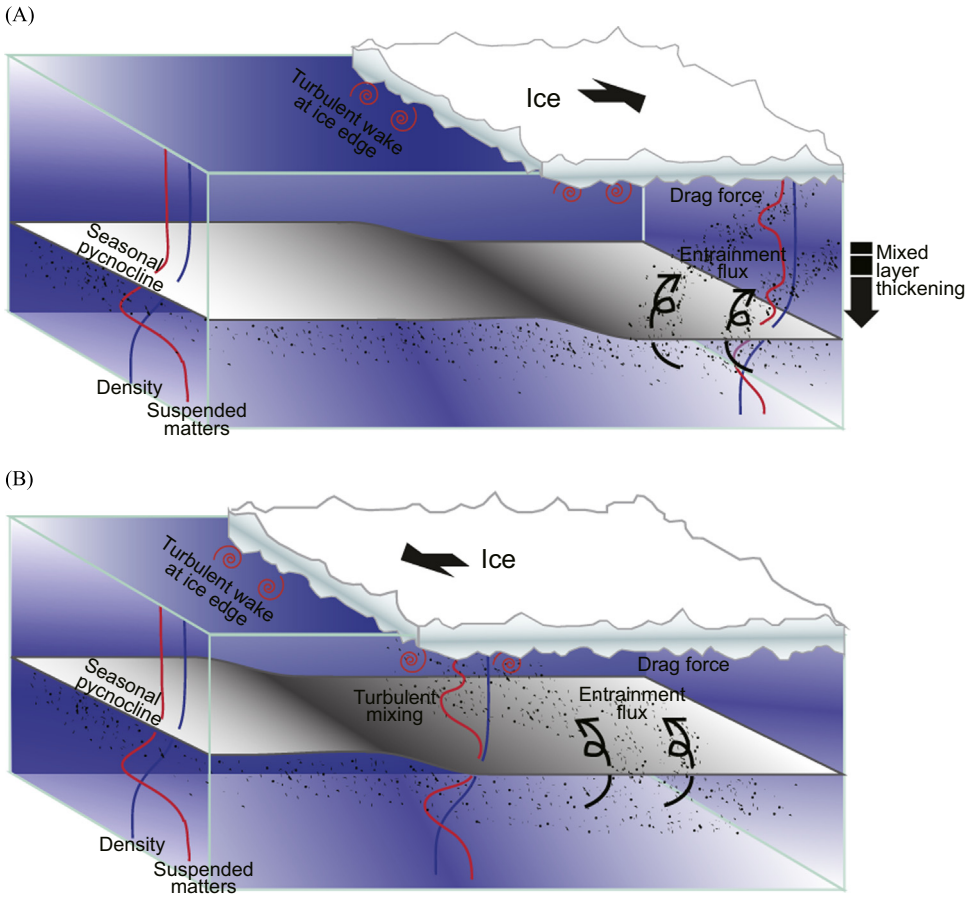

Fig. 9. Schematic diagrams for explaining the entrainment into the upper mixed layer induced by sea ice movement: ice floe drifting to (A) ice pack and (B) lead (open water). (A) Ice floe drifting to ice pack (B) Ice floe drifting to lead (open water).

data from the St. 5-1 through St. 5-3 (taken at 12 – 18 h before ice station) show the uplift of pycnocline from 10 m to 5 m in 6 h. This matches well with vertical oscillation observed in the ice station. It is noted that these stations are approximately 10 km away from the initial ice station, and the hydrographic and hydrodynamic regime would not be much different among stations, considering the inertial excursion of ~7 – 8 km. Morison et al. (1987) reported deepening of the ML from ~10 to 20 m by turbulent entrainment during a storm event. Shoaling of pycnocline by up to 13 m (from 30 to 17 m below the surface) was also observed in the central Arctic Ocean during the SHEBA experiment (McPhee et al., 2005). They suggested that such an event might be associated with large shear in sea ice motion caused by the gradients in large-scale surface wind stress.

The effect of near-inertial oscillation induced by strong wind event was studied by McPhee (1980) using observation data (AIDJEX experiment in the central Arctic during summer of 1975) as well as multi-level, time-dependent dynamical boundary layer simulation. He claimed that the large shear across the pycnocline does not generate enough mixing due to relatively small stress. By comparing turbulent kinetic energy (TKE) production at steady state between hourly and 12-h time scales, he also concluded that the inertial motion is not strong enough to cause a dramatic change in the entrainment rate at the density interface although it may enhance turbulent mixing in the ML. However, his steady-state model did not consider the oscillatory effect that further enhances the entrainment and mixing observed in this study. In fact, Fig. 11 in McPhee (1980) shows the time integrals of shear-produced TKE increased almost twice when considering near-inertial oscillation. McPhee et al. (2003) estimated ocean-to-ice heat flux on a drifting ice station during May 2002 to March 2003. The strong correlation between near-inertial ice drift and heat flux (see Fig. 6 in McPhee et al. (2003)) indicates that shear generated by near-inertial oscillation would enhance the entrainment across the pycnocline, which in turn increases the heat flux. Skyllingstad et al. (2003) found such mixing and entrainment could be enhanced in case of drifting ice with keels, approximately five times larger than the case with flat ice bottom.

In ice-free ocean, the near-inertial oscillations triggered by wind events subside within a few days or weeks mostly due to the internal friction within ML and the radiation of inertial waves toward the pycnocline (Price, 1983; D'Asaro et al., 1995; Garrett, 2001). In ice-covered oceans, however, the inertial oscillation is further damped by internal ice stress, especially in packed winter ice condition. Previous observations have shown that inertial ice motion becomes less frequent when the ice is consolidated together in winter and vice versa (Geiger and Perovich, 2008; Gimbert et al., 2012), and that internal wave (generated by inertial motion) can be damped by internal ice stress through fracturing and crushing (Colony and Thorndike, 1980). Most recently, we witness the dramatic reduction of sea ice extent (Parkinson and Comiso, 2013) and its thinning (Kwok and Rothrock, 2009) in the Arctic Ocean. Such changes are known to correlate with increase in sea ice drift velocity (Rampal et al., 2009; Kwok et al., 2013). Several studies showed an increase of ice drift speed of 9% per decades from 1979 to 2007 (e.g., Rampal et al., 2009), and the positive trends in sea ice drift speed in area of more than 90% of the Arctic Ocean based on the analysis of 1982–2009 data sets (Kwok et al., 2013). Thinning and shrinking trend of sea ice in the Arctic Ocean means more active deformation and inertial motion

even in winter condition (Kwok et al., 2003; Hwang et al., 2015). In this context, our findings imply that more active mixing and entrainment across the pycnocline could supply more heat, salt, and nutrients into the upper ML (i.e., deepening the ML) (McPhee and Martinson, 1994). This means a positive feedback as follows: ice melt→faster ice drift→inertial motion→more upward flux of heat and salt to the ML→enhanced ice melt. This argument is in line with Rainville and Woodgate (2009) and Rainville et al. (2011) who found increased internal wave activity that enhances upper-layer mixing under recent dramatic summer ice retreat. At this juncture, it should be noted that more meltwater from intensive ice melt could stabilize the surface ML, which may cause a negative effect by dissipating internal wave energy in the boundary layer (Guthrie et al., 2013).

4.3. Biogeochemical implications of the entrainment

Beam attenuation data from transmissometer show that a high concentration layer with suspended materials exists right below the seasonal pycnocline at St. 5-1 or even in the ML at St. 5-2 and 5-3 (see Figs. 2 and 3f). Considering that the study area is distant from lateral sources of mineral-origin sediments from continental margins, it is plausible to assume that the materials concentrated in such layers would be produced by local biological processes. Many studies reported that dead organisms after active primary production in the ML settle down to the upper part of pycnocline where water density abruptly changes and thus settling velocity decreases (Wong et al., 1999; Whitney et al., 2013). Ha et al. (unpublished data) also confirmed this argument by analyzing holographic images of suspended particulate materials in the ML.

Our observation is just a few weeks after the experiment described in Arrigo et al. (2012) who reported significant under-ice bloom in the Chukchi Borderland. At most of our stations, increased Chl-*a* concentration was also observed near the upper portion of the permanent pycnocline. As MIZ advances to the north over a few weeks (e.g., Cavalieri et al., 2011), our study area represents environmental conditions (i.e., ice coverage, solar insolation, surface water temperature, and even nutrient distribution) similar to those in Arrigo et al. (2012). One of fundamental differences, however, is that the study area is located distant from the shelf break, and thus the upwelling is not a plausible mechanism to support vertical nutrient mixing from below seasonal pycnocline. It should be noted that no significant Chl-*a* concentration was observed in the surface ML at any of our stations. However, we observed elevated concentration of suspended organic particles in the ML and upper part of seasonal pycnocline, which is comparable to high POC concentration (remaining organic materials of recent under-ice bloom) reported by Arrigo et al. (2012).

During our survey, SCM was clearly observed at the entire stations, which is characterized by high fluorescence signal, high in-situ concentration of Chl-*a*, and high beam attenuation rate. Similar magnitude of elevated beam attenuation was observed in the ML, but it was not accompanied by fluorescence. This indicates that those particles are either lithogenic or photo-physiologically inactive organic matters. Since this area is distant from the source of mineral materials, they are probably organic matters locally produced but no photosynthetically active any more. Then, the question is when they were produced? Authors may speculate that they just bloomed under the ice as Arrigo et al. (2012) suggested, because inactive biogenic materials tend to be settled down out of ML within a reasonable time frame (i.e., several days or weeks). Tremblay et al. (2008) showed the observational evidence for bloom dynamics in early opening waters of the Arctic Ocean. Their results showed that net consumption of nitrate, one of most limiting nutrients in the Arctic Ocean, began at mid-March and it completely depleted in the ML within a month. When inferred from Chl-*a* measurements, it took approximately 3 months (from mid-March through mid-June) between under-ice bloom and onset of SCM. Although their observation was conducted in different regions (i.e., on the continental shelf and 70°N), ice concentration was larger than 90% until June, which is comparable environmental conditions in the surface ML of both Arrigo's and our study areas. Thus, it is reasonable to assume that under-ice bloom initiated on our locations a few months before the observation (see Fig. 1 in Wassmann and Reigstad (2011)). The abundance in particulate materials in the upper ML can increase absorption of shortwave trapping more solar radiant flux in the water column, which will also enhance ice melting (Morel and Antoine, 1994; Perovich and Richter-Menge, 2000; Edwards et al., 2004; Hill, 2008; Paaijmans et al., 2008).

Although observed particulate organic matters are photosynthetically inactive materials, they indicate that there had been under-ice biological activities by phytoplankton in the upper ML until the depletion of nutrients that eventually caused demise of blooms (see Fig. 3). In order to sustain the primary production, favorable light conditions along with episodic but frequent supply of nutrients from the below permanent pycnocline would be essential (Lee and Whitledge, 2005; Lee et al., 2010, 2012; Yun et al., 2012). The supply of nutrients has been attributed to several vertical mixing mechanisms including internal waves, winter storms, tidal mixing, wind-driven upwellings and cyclonic eddies (Reissmann et al., 2009; Popova et al., 2012, 2013). However, none of previous studies has considered entrainment mechanism induced by near-inertial ice motion discussed in this study. Although our study presents evidence that can explain only the case of the seasonal pycnocline, the dynamics could well be extended to deeper permanent pycnocline where higher concentration of nutrients is present if a stronger wind event occurs. When we have a strong storm event, the storm itself stirs and mixes water column vertically but also it triggers a strong ice drift motion which may continue for next several weeks. This inertial drift derived by strong wind events may deliver intensive and continuous mixing and entrainment in the water column via processes discussed in this study. This is in line with Geiger and Perovich's (2008) suggestion that the inertial sea ice motion might serve as an effective seeding platform for distributing phytoplankton and zooplankton overwintering around the ice floes.

5. Conclusions

Mixing and entrainment mechanisms in the upper ML of the MIZ were evaluated by analyzing the data of hydrodynamics, hydrography and suspended particles measured on a drifting ice station. The results revealed direct and indirect evidences of mixing and entrainment pattern in the ML as well as across the upper part of seasonal pycnocline. Echo intensity (proxy of suspended particles) from ADCP showed both upward and downward fluxes of the particulate materials over two near-inertial periods. The thickness of ML, observed by CTD, oscillated with the near-inertial period whereby thickening during accelerating period and vice versa. The thickness of the ML inferred from the velocity shear was also consistent with what was measured by CTD.

The mixing and entrainment pattern can be divided into two regimes during each near-inertial drift period. In the first regime when the sea ice drifts toward pack ice and ice drift speed accelerates, shear across the pycnocline enhances entrainment whilst turbulent wake occurs behind the advancing edge of ice, resulting in simple upward fluxes (entrainment) from the pycnocline to sea ice–water boundary. In the second regime when the

sea ice drifts toward open ocean (i.e., lead), the turbulent wake at the advancing edge of ice combines with the entrainment caused by near-inertial motion, resulting in complex mixing patterns. This oscillatory mixing induced by near-inertial drift has not been significantly considered in the modeling efforts of the Arctic Ocean. Recent extensive summer sea-ice retreat would increase ice drift speed and inertial motion, which in turn enhances mixing and entrainment across the pycnocline that was observed in our study. This will entrain more heat to the ice–water boundary, which will act as positive feedback in ice melting mechanism.

Our observation provides 3-D mapping of particle entrainment in the ML. The active inertial motion of sea ice can entrain warmer water, particulate matters as well as other dissolved materials into the ML, which may sustain elevated concentration of organic matters for relatively long period (e.g., a few months). This was confirmed by elevated beam attenuation not only in ice station, but also all stations in the central Arctic Ocean. Once it is accompanied by under-ice bloom, the abundant organic particulates after the bloom would be suspended in the upper ML. More particulate organic materials in the upper ML also enhance absorption of solar radiant flux, which subsequently changes thermal structure in the upper Arctic Ocean in addition to heat flux from entrained warm seawater.

Acknowledgments

The authors are grateful to the enthusiastic support of the captain and crews of IBRV Araon during the ARA02B cruise. This research was a part of the project titled “K-PORT (KOPRI, PM13020)”, funded by the MOF, Korea. HKH was supported by Inha University Research Grant (INHA-49278) and KOPRI Polar Academic Program (PD14010), and YHK and JHP was supported by the MOF, Korea through a Grant “Development of Satellite based Ocean Carbon Flux Model for Seas around Korea”.

References

Aagaard, K., Coachman, L.K., Carmack, E.C., 1981. On the halocline of the Arctic Ocean. Deep Sea Res. 28, 529–545.

Arrigo, K.R., Perovich, D.K., Pickart, R.S., Brown, Z.W., van Dijken, G.L., Lowry, K.E., Mills, M.M., Palmer, M.A., Balch, W.M., Bahr, F., Bates, N.R., Benitez-Nelson, C., Bowler, B., Brownlee, E., Ehn, J.K., Frey, K.E., Garley, R., Laney, S.R., Lubelczyk, L., Mathis, J., Matsuoka, A., Mitchell, B.G., More, G.W.K., Ortega-Retuerta, E., Pal, S., Polashenski, C.M., Reynolds, R.A., Schieber, B., Sosik, H.M., Stephens, M., Swift, J. H., 2012. Massive phytoplankton blooms under Arctic sea ice. Science 336, 1408, http://dx.doi.org/10.1126/science.1215065.

Carmack, E., Melling, H., 2011. Warmth from the deep. Nat. Geosci. 4, 7–8.

Cavalieri, D., Markus, T., Comiso, J., 2011. AMSR-E/Aqua Daily L3 12.5 km Brightness Temperature, Sea Ice Concentration, and Snow Depth Polar Grids V002. National Snow and Ice Data Center. Digital Media, Boulder, Colorado, USA.

Colony, R., Thorndike, A., 1980. The horizontal coherency of the motion of summer Arctic sea ice. J. Phys. Oceanogr. 10, 1281–1289.

D’Asaro, E.A., Eriksen, C.C., Levine, M.D., Niiler, P., Paulson, C.A., Meurs, P.V., 1995. Upper-ocean inertial currents forced by a strong storm. Part I: Data and comparisons with linear theory. J. Phys. Oceanogr. 25, 2909–2936.

Edwards, A.M., Wright, D.G., Platt, T., 2004. Biological heating effect of a band of phytoplankton. J. Mar. Syst. 49, 89–103.

Fer, I., Sundfjord, A., 2007. Observation of upper ocean boundary layer dynamics in the marginal ice zone. J. Geophys. Res. 112, C04012, http://dx.doi.org/10.1029/2005JC003428.

Garrett, C., 2001. What is the “near-inertial” band and why is it different from the rest of the internal wave spectrum? J. Phys. Oceanogr. 31, 962–971.

Geiger, C., Perovich, D., 2008. Springtime ice motion in the Western Antarctic Peninsula region. Deep-Sea Res. II 55, 338–350.

Gimbert, F., Jourdain, N.C., Marsan, D., Weiss, J., Barnier, B., 2012. Recent mechanical weakening of the Arctic sea ice cover as revealed from larger inertial oscillations. J. Geophys. Res. 117, C00J12, http://dx.doi.org/10.1029/2011JC007633.

Guthrie, J.D., Morison, J.H., Fer, I., 2013. Revisiting internal waves and mixing in the Arctic Ocean. J. Geophys. Res. 118, 3966–3977, http://dx.doi.org/10.1002/jgrc.20294.

Ha, H.K., Kim, Y.H., Lee, H.J., Hwang, B., Joo, H.M., Measurement of suspended particulate matter under Arctic sea ice during the rapidly-melting summer season. unpublished data.

Hill, V.J., 2008. Impacts of chromophoric dissolved organic material on surface ocean heating in the Chukchi Sea. J. Geophys. Res. 113, C07024, http://dx.doi.org/10.1029/2007JC004119.

Holland, M.M., 2003. An improved single-column model representation of ocean mixing associated with summertime leads: results from a SHEBA case study. J. Geophys. Res. 108, 3107, http://dx.doi.org/10.1029/2002JC001557.

Hwang, B.J., Wilkinson, J., Elosegui, P., 2015. Small-scale deformation of an Arctic sea ice floe detected by GPS and satellite imagery. Deep Sea Res. II 120, 3–20, http://dx.doi.org/10.1016/j.dsr2.2015.01.007.

Kato, H., Phillips, O., 1969. On the penetration of a turbulent layer into stratified fluid. J. Fluid Mech. 37, 643–655.

Kranenburg, C., 1984. Wind-induced entrainment in a stable stratified fluid. J. Fluid Mech. 145, 253–273.

Kwok, R., Cunningham, G.F., Hibler III, W.D., 2003. Sub-daily sea ice motion and deformation from RADARSAT observation. Geophys. Res. Lett. 30, 2218, http://dx.doi.org/10.1029/2023GL018723.

Kwok, R., Rothrock, D.A., 2009. Decline in Arctic sea ice thickness from submarine and ICESat records: 1958–2008. Geophys. Res. Lett. 36, L15501, http://dx.doi.org/10.1029/2009GL039035.

Kwok, R., Spreen, G., Pang, S., 2013. Arctic sea ice circulation and drift speed: decadal trends and ocean currents. J. Geophys. Res. 118, 2408–2425.

Lee, S.H., Joo, H.M., Liu, Z., Chen, J., He, J., 2012. Phytoplankton productivity in newly opened waters of the Western Arctic Ocean. Deep-Sea Res. II 81–84, 18–27.

Lee, S.H., Stockwell, D., Whitledge, T.E., 2010. Uptake rates of dissolved inorganic carbon and nitrogen by under-ice phytoplankton in the Canada Basin in summer 2005. Polar Biol. 33, 1027–1036.

Lee, S.H., Whitledge, T.E., 2005. Primary and new production in the deep Canada Basin during summer 2002. Polar Biol. 28, 190–197.

McPhee, M.G., 1978. A simulation of inertial oscillation in drifting pack ice. Dyn. Atmos. Oceans 2, 107–222.

McPhee, M.G., 1980. A study of oceanic boundary-layer characteristics including inertial oscillation at three drifting stations in the Arctic Ocean. J. Phys. Oceanogr. 10, 870–884.

McPhee, M.G., 1983. Turbulent heat and momentum transfer in the oceanic boundary layer under melting pack ice. J. Geophys. Res. 88, 2827–2835.

McPhee, M.G., 1987. A time-dependent model for turbulent transfer in a stratified oceanic boundary layer. J. Geophys. Res. 92, 6977–6986.

McPhee, M.G., 1992. Turbulent heat flux in the upper ocean under sea ice. J. Geophys. Res. 97, 5365–5379.

McPhee, M.G., 1994. On the turbulent mixing length in the oceanic boundary layer. J. Geophys. Res. 24, 2014–2031.

McPhee, M.G., 2002. Turbulent stress at the ice/ocean interface and bottom surface hydraulic roughness during the SHEBA drift. J. Geophys. Res. 107, 8037, http://dx.doi.org/10.1029/2000JC000633.

McPhee, M.G., 2004. A spectral technique for estimating turbulent stress, scalar flux magnitude, and eddy viscosity in the ocean boundary layer under pack ice. J. Geophys. Res. 34, 2180–2188.

McPhee, M.G., Kikuchi, T., Morison, J.H., Stanton, T.P., 2003. Ocean-to-ice heat flux at the North Pole environmental observatory. Geophys. Res. Lett. 30, 2274, http://dx.doi.org/10.1029/2003GL018580.

McPhee, M.G., Kwok, R., Robins, R., Coon, M., 2005. Upwelling of Arctic pycnocline associated with shear motion of sea ice. Geophys. Res. Lett. 32, L10616, http://dx.doi.org/10.1029/2004GL021819.

McPhee, M.G., Martinson, D.G., 1994. Turbulent mixing under drifting pack ice in the Weddell Sea. Science 263, 218–221.

McPhee, M.G., Maykut, G.A., Morison, J.H., 1987. Dynamics and thermodynamics of the ice/upper ocean system in the marginal ice zone of the Greenland Sea. J. Geophys. Res. 92, 7017–7031.

McPhee, M.G., Stanton, T.P., 1996. Turbulence in the statically unstable oceanic boundary layer under Arctic leads. J. Geophys. Res. 101, 6409–6428.

Morel, A., Antoine, D., 1994. Heating rate within the upper ocean in relation to its bio-optical state. J. Phys. Oceanogr. 24, 1652–1665.

Morison, J.H., McPhee, M.G., Maykut, G.A., 1987. Boundary layer, upper ocean, ice observations in the Greenland Sea Marginal ice zone. J. Geophys. Res. 92, 6987–7011.

Mundy, C.J., Gosselin, M., Ehn, J., Gratton, Y., Rossnagel, A., Barber, D.G., Martin, J., Tremblay, J.E., Palmer, M., Arrigo, K., Darnis, G., Fortier, L., Else, B., Papakyriakou, T., 2009. Contribution of under-ice primary production to an ice-edge upwelling phytoplankton bloom in the Canadian Beaufort Sea. Geophys. Res. Lett. 36, L17601, http://dx.doi.org/10.1029/2009GL038837.

Nagai, T., Yamazaki, H., Nagashima, H., Kantha, L.H., 2005. Field and numerical study of entrainment laws for surface mixed layer. Deep-Sea Res. II 52, 1109–1132.

Narimousa, S., Long, R.R., Kitaigorodskii, S.A., 1986. Entrainment due to turbulent shear flow at the interface of a stably stratified fluid. Tellus 38A, 76–87.

Paaijmans, K.P., Takken, W., Githeko, A.K., Jacobs, A.F.G., 2008. The effect of water turbidity on the near-surface water temperature of larval habitats of the malaria mosquito Anopheles gambiae. Int. J. Biometeorol. 52, 747–753.

Parkinson, C.L., Comiso, J.C., 2013. On the 2012 record low Arctic sea ice cover: combined impact of preconditioning and an August storm. Geophys. Res. Lett. 40, 1356–1361, http://dx.doi.org/10.1002/grl.50349.

Parsons, T.R., Maita, Y., Lalli, C.M., 1984. A Manual of Chemical and Biological Methods for Seawater Analysis. Pergamon Press, Toronto p. 173.

Perovich, D.K., Richter-Menge, J.A., 2000. Ice growth and solar heating in springtime leads. J. Geophys. Res. 105, 6541–6548.

Popova, E.E., Yool, A., Coward, A.C., Akesenov, Y.K., Alerson, S.G., de Cuevas, B.A., Anderson, T.R., 2010. Control of primary production in the Arctic by nutrients and light: insights from a high resolution ocean general circulation model. Biogeosciences 7, 3569–3591.

Popova, E.E., Yool, A., Coward, A., Dupont, F., Deal, C., Eliott, S., Hunke, E., Jin, M., Stelle, M., Zhang, J., 2012. What controls primary production in the Arctic Ocean? Results from an intercomparison of five general circulation models with biogeochemistry. J. Geophys. Res. 117, C00D12, http://dx.doi.org/10.1029/2011JC007112.

Popova, E.E., Yool, A., Aksenov, Y., Coward, A.C., 2013. Role of advection in Arctic Ocean lower trophic dynamics: a modeling perspective. J. Geophys. Res. 118, 1571–1586.

Price, J.F., 1979. On the scaling of stress-driven entrainment experiments. J. Fluid Mech. 90, 582–599.

Price, J.F., 1983. Internal wave wake of a moving storm. Part I: scales, energy budget and observations. J. Phys. Oceanogr. 13, 949–965.

Rainville, L., Lee, C.M., Woodgate, R.A., 2011. Impact of wind-driven mixing in the Arctic Ocean. Oceanography 24, 136–145.

Rainville, L., Woodgate, R., 2009. Observations of internal wave generation in the seasonally ice-free Arctic. Geophys. Res. Lett. 36, L23604, http://dx.doi.org/10.1029/2009GL041291.

Rampal, P., Weiss, J., Marsan, D., 2009. Positive trend in the mean speed and deformation rate of Arctic sea ice, 1979–2007. J. Geophys. Res. 114, C05013, http://dx.doi.org/10.1029/2008JC005066.

Reissmann, J.H., Burchard, H., Feistel, R., Hagen, E., Lass, H.U., Mohrholz, V., Nausch, G., Umlauf, L., Wieczorek, G., 2009. Vertical mixing in the Baltic Sea and consequences for eutrophication – a review. Prog. Oceanogr. 82, 47–80.

Rudels, B., Anderson, L.G., Jones, E.P., 1996. Formation and evolution of the surface mixed layer and the halocline of the Arctic Ocean. J. Geophys. Res. 101, 8807–8821.

SAMS, 2010. SIMBA User Guide: SAMS Thermometer Chain based Ice-Mass Balance Array. Scottish Association of Marine Science, Oban (25 pp.).

Shaw, W.J., Stanton, T.P., McPhee, M.G., Morison, J.H., Martinson, D.G., 2009. Role of the upper ocean in the energy budget of Arctic sea ice during SHEBA. J. Geophys. Res. 114, C06012, http://dx.doi.org/10.1029/2008JC004991.

Skyllingstad, E.D., Denbo, D.W., 2001. Turbulence beneath sea ice and leads: a coupled sea ice/large eddy simulation study. J. Geophys. Res. 106, 2477–2497.

Skyllingstad, E.D., Paulson, C.A., Peague, W.S., McPhee, M.G., Stanton, T., 2003. Effects of keels on ice bottom turbulence exchange. J. Geophys. Res. 108, 3372, http://dx.doi.org/10.1029/2002JC001488.

Smith Jr., W.O., Nelson, D.M., 1985. Phytoplankton bloom produced by a receding ice edge in the Ross Sea: spatial coherence with the density field. Science 227, 163–166.

Smith Jr., W.O., Nelson, D.M., 1986. Importance of ice edge phytoplankton blooms in the Southern Ocean. Bioscience 36, 251–257.

Smith Jr., W.O., Niebauer, H.J., 1993. Interactions between biological and physical processes in Arctic Seas: investigations using numerical models. Rev. Geophys. 31, 189–209.

Strang, E.J., Fernando, H.J., 2001. Entrainment and mixing in stratified shear flows. J. Fluid Mech. 428, 349–386.

Toole, J.M., Timmemans, M.L., Perovich, D.K., Krishfield, R.A., Proshutinsky, A., Richter-Menge, J.A., 2010. Influences of the ocean surface mixed layer and thermohaline stratification on Arctic Sea ice in the central Canada Basin. J. Geophys. Res. 115, C10018, http://dx.doi.org/10.1029/2009JC005660.

Tremblay, J.E., Michel, C., Hobson, K.A., Gosselin, M., Price, N., 2006. Bloom dynamics in early opening waters of the Arctic Ocean. Limnol. Oceanogr. 51, 900–912.

Tremblay, J.E., Simpson, K., Martine, J., Miller, L., Gratton, Y., Barber, D., Price, N.M., 2008. Vertical stability and the annual dynamics of nutrients and chlorophyll fluorescence in the coastal, southeast Beaufort Sea. J. Geophys. Res. 113, C07S90, http://dx.doi.org/10.1029/2007JC004547.

Wassmann, P., Reigstad, M., 2011. Future Arctic Ocean seasonal ice zones and implications for pelagic-benthic coupling. Oceanography 24, 220–231.

Whitney, F.A., Bograd, S.J., Ono, T., 2013. Nutrient enrichment of the subarctic Pacific Ocean pycnocline. Geophys. Res. Lett. 40, 2200–2205.

Williams, W.J., Carmack, E.C., 2008. Combined effect of wind-forcing and isobath divergence on upwelling at Cape Bathurst, Beaufort Sea. J. Mar. Res. 66, 645–663.

Wong, C.S., Whitney, F.A., Crawford, D.W., Iseki, K., Matear, R.J., Johnson, W.K., Page, J.S., Timothy, D., 1999. Seasonal and interannual variability in particle fluxes of carbon, nitrogen and silicon from time series of sediment traps at Ocean Station P, 1982–1993: relationship to changes in subarctic primary productivity. Deep-Sea Res. Part II 46, 2735–2760.

Yun, M.S., Chung, K.H., Zimmermann, S., Zhao, J., Joo, H.M., Lee, S.H., 2012. Phytoplankton productivity and its response to higher light levels in the Canada Basin. Polar Biol. 35, 257–268.